ISIJ International, Vol. 41 (2001), No. 6, pp. 626–640

Review

Design of Ferritic Creep-resistant Steels

H. K. D. H. BHADESHIA

Department of Materials Science and Metallurgy, University of Cambridge, Pembroke Street, Cambridge, UK.

(*Received on September 1, 2000; accepted in final form on October 27, 2000*)

Creep resistant steels must be reliable over very long periods of time in severe environments. Their microstructures have to be very stable, both in the wrought and in the welded states. This paper reviews the quantitative methods for the design of steels for elevated temperature applications. A methodology is described for the calculation of complex precipitation reactions over periods extending many tens of years. However, microstructure alone is not enough in the design of alloys. The estimation of the creep rupture stress using a neural network technique is described in the second part of this review. The calculation of the influence of solute-elements on the self-diffusivity of iron, which features in many creep equations, is an emerging area in alloy design. The methodology for such calculations is reviewed in the final section of the paper.

KEY WORDS: creep strength; power plant; carbides; martensite; bainite.

1. Introduction

The efficiency of steam turbines can be improved by increasing the maximum operating pressure and temperature. The efficiency describes the proportion of the energy that is fed in, for example by burning coal, that is converted into electricity. A greater efficiency leads to a saving in fuel for a given electricity output with a consequential reduction in the rate at which damage is done to the earth's environment. The purpose of this paper is to review the quantitative methods that are currently available for the invention of new steels capable of sustaining the higher temperatures envisaged for high-efficiency power plant.

2. Turbines, Steam, Efficiency and Power Plant

A power plant has a steam generator which is a facility for producing superheated steam at very high pressures. Liquid water and steam can coexist when the operating pressure is below about 22 MPa, in which case the steam is separated and passed on to the turbine generator. The turbine works on the Parsons' principle, that the fall in pressure of the steam should occur in small fractional expansions over a large number of blades in series, so that the velocity of the steam nowhere should be great. Naturally, the volume of the steam gradually increases with the successive reduction in pressure. Succeeding turbines are therefore larger in terms of the blade height and diameter. Many modern turbine generators have three distinct stages, the high pressure (HP) turbine where the high-pressure steam from the boiler does its work and in so doing, reduces in pressure and temperature. The steam is then sent to a reheater to return to an intermediate pressure (IP) turbine. The steam that exits the IP turbine goes into the low-pressure (LP) turbine where it is expanded down to the pressure appropriate for the condenser (**Table 1**).

There are now more than 400 power plant in the world which operate on somewhat different (supercritical) conditions than those outlined in Table 1. In particular, the pressure is raised to a value greater than 22 MPa. There is then no distinction between the liquid and gaseous states of water. In normal circumstances, a gas has a high compressibility and on changing to a liquid the compressibility abruptly decreases. With a supercritical fluid, the compressibility decreases monotonically as the volume is reduced. From the point of view of power plant the supercritical conditions lead to higher efficiency simply because the steam pressure and possibly temperature is higher; the state of the fluid does not seem to affect the efficiency calculations. There are nevertheless engineering consequences; for example, the boiler need no longer have a system to separate water and steam, since there is only one fluid.

A typical subcritical power plant may at installation have an efficiency approaching 40 %. The use of high pressure (30 MPa) in a supercritical plant can raise this to 45 %. If the steam temperature is also increased (ultra supercritical conditions) then efficiencies of 50 % are possible.

3. Engineering Requirements

This elementary introduction to electricity generation is

Table 1. An example of steam conditions in a turbine generator set. The terms HP, IP and LP stand respectively for high pressure, intermediate prssure and low pressure stage of the turbine set.

Stage	Entry pressure and temperature		Exit pressure and temperature	
HP	16 MPa	565 °C	4 MPa	420 °C
IP	4 MPa	565 °C	0.6 MPa	250 °C
LP	0.6 MPa	250 °C	0.1 MPa	100 °C

intended to set the scene for a discussion of the materials associated with the construction of reliable boilers and turbines. The properties required by the turbine design engineer for the construction of reliable boilers and turbines have been listed and succinctly described by Thornton and Mayer.[2] Many of the components have to support loads at elevated temperatures; this causes thermally activated, slow and continuous plastic strain which increases with time. For well-designed materials, this creep strain will be tolerable over the design life of the component. The engineer has to be reassured that the creep will not cause rupture or unacceptable dimensional changes. A typical tolerable creep strain rate may be about $3\times10^{-11}\,s^{-1}$, or approximately 2 % elongation over 30 years. It is also common to specify that the material must be able to support a stress of 100 MPa at service-temperature over a time period of 10^5 h without fracture. When fracture does eventually occur, it must be associated with a certain amount of creep ductility. In the case of bolting, the relaxation of the bolting stress by creep determines the sealing life.

Engineering components, especially large ones, always contain defects. The important point is not the existence of these defects but that they must not be large enough to propagate rapidly and hence cause catastrophic failure. Knott[3] calls the fast propagating crack, the "crack of doom". To avoid such condemnation, any proposed material must have a certain fracture toughness which defines its ability to tolerate defects. Any defect present when the component enters service can grow slowly and eventually reach a critical size where it propagates catastrophically. The most frequent cause of slow crack growth is exposure to cyclic stresses but in power plant the problem can be exacerbated by the combined action of stress and temperature fluctuations. There are generally two different frequencies of loading to consider: low cycle fatigue occurs due to discontinuous operation, whereas high cycle fatigue is by the cyclic motion of components.

Many components have to be joined by welding. The gap between the parts to be joined is filled with molten metal which then solidifies giving an integral joint. It is amazing that we dare to do this to engineering components. For welding is perhaps the most complex of fabrication processes, embodying virtually every metallurgical phenomenon: solidification, solid-state phase transformations, heat treatment, residual stress development and subtle chemical composition effects. Not only are the properties of the weldment expected to be different from those of the components to be joined, but the flow of heat into the solid components causes metallurgical changes which can make or break the joint in the critical heat affected zone adjacent to the fusion boundary. Thornton and Mayer describe the requirements of a welded joint by an all encompassing term, the weldment life.

There are many other properties to consider: oxidation and corrosion resistance, time-dependent impurity effects, hardenability, castability, forgeability and many other abilities.[4–8]

4. The Task

Given the formidable engineering requirements, the metallurgist's task is as follows. Metals are made of atoms and may contain molecules; the constituent atoms can be anything in the periodic table and beyond[9]; one or more species of atoms can be arranged in many ways to form patterns. As with wallpaper, each of these patterns can be represented by a unit of the pattern, the unit cell, and a motif of atoms associated with each cell, to form the crystal structure. The distribution of atoms in a macroscopic crystal can be described in terms of the three-dimensional stacking of these unit cells containing the motif of atoms. The macroscopic shape of the crystal depends on the environment, processing and many other factors determined mostly by the fact that a lump of metal is generally polycrystalline and is filled completely with many millions of one or more kinds of crystals. The fact that the lump of metal is a conglomerate of crystals is frequently hidden from view so an engineer may treat the metal as a continuum. There is another complication. Nothing in nature is perfect; indeed, equilibrium demands that crystals should be imperfect. Metals may not be as useful as they are without certain defects; hence the phrase, "the importance of being imperfect".[10] For example, there is always an equilibrium concentration of point defects. More significant are the nonequilibrium, unintended defects introduced in the process of manufacture. This paragraph begins with atoms, but electrons must feature in any description of the state of matter, for they form the bonds between atoms.

These are the factors which affect the nature and properties of materials. The theme of this paper is the design of heat-resistant alloys, with the implication that it would be wonderful to be able to make the alloy manufacturing specification emerge from calculations, as apparently did Parson's steam turbine.[1] This is in contrast to the alternative method, in another field known as combinatorial chemistry, where a large number of experiments are conceived using intuition in the hope that something works.

Unfortunately, it is unlikely that there can ever be a unifying theory which takes all the scales of defect-rich structure into account and permits the design of an alloy that satisfies the criteria stated by Thornton, Mayer and others. The task is simply too complicated, the knowledge too sparse and the application too critical. There could be life-threatening consequences in the event of failure. To paraphrase a nuclear physicist,[9] we only have models which give a good description of particular phenomena over a restricted range of parameters.

Some might take this to be a pessimistic view, but the formidable problems are frequently the ones that are the most exciting — this is part of the reason why some scientists pursue careers on the stock exchange. The important point is that there must be tangible progress in the theories so that the use of resources is optimised. Though it is not yet possible to avoid experiments, the experiments performed can be defined better by calculation. I shall summarise the performance of current alloy design procedures, outline the outstanding problems and give examples of alloys which have emerged through the combined use of theory and experiments.

5. Electrons, Bonds, Creep and Carbides

The atoms in a metal are held together by a special gas of free electrons which allows the ensemble to bond even when different kinds of atoms are put together in solid solution.[11] There is theory to enable electron densities and total energies to be estimated using only the atomic number and the charge on the electron.[12] The methodology is particularly useful in the prediction of crystal structure, elastic moduli and surface energies.

There is a limitation in that the technique is computer intensive so it must deal with small numbers of atoms, which in practice means a representative unit cell. It then becomes difficult to handle disordered solid solutions, although some parameters can be derived which may be of use in thermodynamic models of phase diagrams.[13]

There have been applications of electron theory to the specific problem of the creep rupture strength of ferritic steels. Morinaga and co-workers[14,15] have used a molecular orbital method to calculate two parameters, the bond-order B_O and M_d to suggest trends in creep-resistant steels. The bond order represents the number of electrons in bonding orbitals less those in anti-bonding ones.[16] For a pair of atoms, an anti-bonding orbital is one where the electron density falls to zero at some point between the adjacent atomic nuclei. A weaker bond thus has a lower bond order; bonding is absent when the bond order is 0.*1 In the present context B_O represents a major contribution to the strength of the bond between a solute and iron atom in the body-centred cubic (b.c.c.) crystal structure. The parameter M_d correlates with electronegativity and the atomic radius of the element concerned. Values of these two parameters for a number of common solutes in ferrite are shown in **Fig. 1**.

The natural question to ask is what does bond strength and electronegativity have to do with creep deformation, which depends on the ability of dislocations to overcome obstacles by thermally activated climb? The answer has to be that there is no physical basis for using either B_O or M_d in design against creep, but Morinaga claims that there is an empirical correlation between the creep rupture strength and the mean bond order of a commercial steel as long as the latter is free from δ-ferrite (**Fig. 2**); furthermore, M_d correlates directly with the propensity to form δ-ferrite in the steels studied. He suggest that the method can be used to optimise steels by maximising B_O and minimising M_d. This was demonstrated by making appropriate additions to the commercial alloy NF616 (**Table 2**).[14]

It could be argued that the results presented in Table 2 validate the use of the molecular orbital approach in the design of steels. However, a closer study of the data casts doubt on the procedure. For example, tungsten has a significantly larger B_O than rhenium, and furthermore, it is known that larger concentrations of tungsten can be tolerated in balanced alloys without introducing δ-ferrite or Laves phases.[17] The addition of rhenium is not justified by the molecular orbital calculations, but as admitted in the paper, has been made because rhenium is known to improve the creep properties of nickel base superalloys. Cobalt has a lower B_O than iron, so its addition is only justified to balance the tendency for chromium at high concentrations to promote δ-ferrite. To summarise, neither the rhenium nor the cobalt modifications of NF616 are based on the molecular orbital calculations but rather on intuition and knowledge as reported in the literature. Similar comments can be made about a later paper[15] in which the method was used to develop rotor steels. The case that the molecular orbital calculations have predictive power has not in my opinion

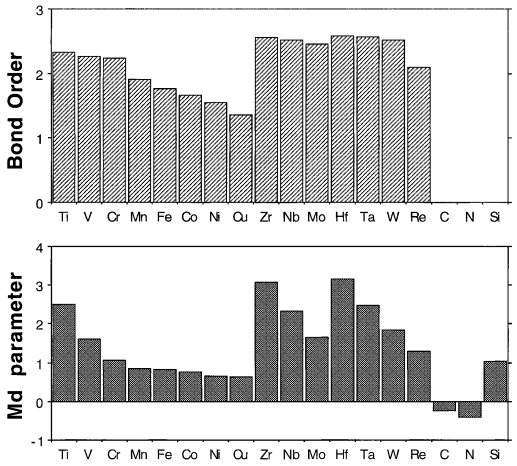

Fig. 1. The bond order and M_d parameter for a number of solutes in body-cented cubic iron.[14,15]

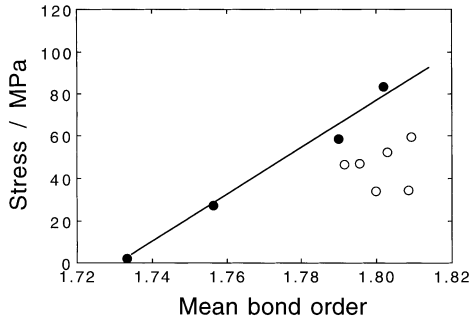

Fig. 2. The correlation of the allowable stress at 600 °C against the mean bond order of a variety of commercial steels. The open circles represent alloys which may contain some δ-ferrite whereas those which are filled represent δ-ferrite-free steels.[14]

Table 2. Compositions (wt%) of steels studied by Morinaga *et al.*[14] All nominally contain 0.07C, 0.06Si, 0.45Mn, 0.5Mo, 0.2V, 0.05Nb, 0.01Al, 0.004B and 0.06N wt%, so the compositions stated are presumably nominal. The final column gives the time to creep rupture at 700°C for a stress of about 8 MPa.

Alloy	Cr	W	Co	Re	time / h
NF616	9.0	1.8	0.0	0.0	406
B1	10.0	1.8	1.5	0.0	919
B2	10.0	1.5	1.5	0.6	1103
B3	11.5	1.8	2.5	0.0	1024
B4	11.5	1.5	2.5	0.6	1263

*1 When two hydrogen atoms, each with a single electron, are brought together, they no longer have separate atomic orbitals. Instead they have a pair of communal orbitals (bonding and antibonding) each of which can hold two electrons. It follows that for H_2 both the electrons are in the bonding orbitals giving a bond order of 2 and a strong molecule. For He_2, on the other hand, the four electrons fill up both the bonding and antibonding orbitals so the bond order is zero, the molecule is not formed.[16]

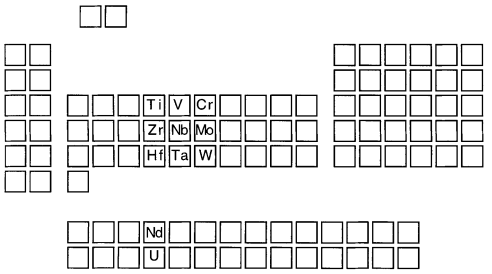

Fig. 3. The periodic table showing the positions of strong carbide-forming elements.

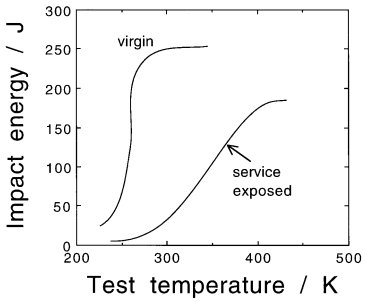

Fig. 4. Impact test data on 2¼Cr1Mo steel. Comparison of the impact energies of the steel in its virgin condition, after service exposure at 813 K for 88 000 h. After Wignarajah *et al.*[26]

been made. Nor is it obvious why such a method should work when creep rupture is controlled by defects and precipitates on a scale many millions of times larger than atoms.

Carbides

Perhaps a better way to use the concepts of chemical bonding would be to examine the stabilities of the precipitates which strengthen steels. Cottrell[16] has been able to explain many of the observed trends in the stability, crystal structure and stoichiometry of the carbides of transition metals in terms of chemical bonds. He points out that Ti, Zr and Hf, which in the periodic table are elements near the beginning of the long periods, form very stable MC carbides but the affinity for carbon diminishes further along the rows of the periodic table (**Fig. 3**). A part of the reason for this is that more electrons have to be accommodated for elements further along the rows, so antibonding states are progressively filled thereby reducing the bond order. This is analogous to the hydrogen–helium example given earlier, but does not completely explain the trend because the maximum bond order occurs with Cr, Mo and W and we know that carbides of these elements are less stable.

With MC carbides, the metal has to sacrifice four electrons to form the bonds with carbon. Titanium has exactly the right number so that its *d*-orbitals are left empty on forming TiC. This is not the case with VC, since vanadium has an additional *d*-electron which forms a V–V bond. The electrons in the two kinds of bonds, V–C and V–V mutually repel, leading to a reduction in the stability of VC when compared with TiC. This problem becomes larger along the row of the periodic table until MC carbide formation becomes impossible or unlikely.

Although Cottrell has not considered the carbides in the lanthanide or actinide series of elements, it is possible that the same principles should apply there. Both NdC and UC exist. Remarkably, neodynium nitride has already been incorporated into a ferritic creep-resistant steel by Igarashi and Sawaragi[18] with rather good results. The concentration of neodynium used was only 0.04 wt% but gave an increase in the creep rupture life by a factor of about two during tests at 650 °C. They also tried hafnium but did not recommend it due to a tendency to form coarse particles.

6. Embrittlement and Electron Theory

Impurity-induced embrittlement is a severe problem in the power generation industries, both at the fabrication stage and as we shall see later, the toughness deteriorates during prolonged service at elevated temperatures.

Grain Boundary Embrittlement

Modern creep-resistant steels begin with a martensitic microstructure. Martensitic transformation occurs with the disciplined motion of atoms. Such movements cannot be sustained across grain boundaries. It follows that a vestige of the austenite grain boundary remains when the transformation is displacive. These prior boundaries become susceptible to impurity segregation and embrittlement, liquid zinc embrittlement, and any phenomenon able to exploit the disorder associated with these boundaries.[19–22]

The disorder at the prior austenite grain boundaries is larger than that associated with martensite–martensite boundaries. This is because adjacent martensite plates have coherence with the parent austenite grain and hence a good fit with each other, whereas the orientation relationships between austenite grains can be random. There are considerable practical consequences of this difference. Thus, the extent of segregation is smaller at martensite lath boundaries. Carbides nucleate preferentially at the prior austenite grain boundaries during the tempering of martensite or bainite.[23,24] The boundaries can be revealed by etching,[25] often with great clarity even though the original grain is no longer present.

The problem of austenite grain boundary embrittlement in martensitic or bainitic steels is not exclusive to high strength steels used at ambient temperature. It is well established that the fracture toughness of many power plant steels deteriorates during service at elevated temperatures for two reasons. Firstly, the carbide particles, particularly those located at the prior boundaries, coarsen and hence provide easier sites for crack or void nucleation. Secondly, the elevated temperatures permit the impurities to diffuse relatively rapidly and saturate the boundaries. **Figure 4** shows the impact transition curves for both the virgin steel (*i.e.* at implementation into service) and for an ex-service sample which had experienced 88 000 h at 813 K.[26]

Mechanism of Embrittlement

Rice and Wang's theory[27] defines the impurity effect precisely: embrittlement occurs if the magnitude of the reduction ΔG_b in free energy which occurs when an impurity segregates to a grain boundary is less than when the impurity segregates to a free surface (ΔG_s). This is because the impurity then prefers to be at a free surface than at a boundary. **Table 3** lists some values for these terms for a number

Table 3. The free energies of segregation to a grain boundary and to a free surface. These values must naturally depend on factors such as the grain boundary structure—the details can be found in Ref. 27).

Segregant	$-\Delta G_b$	$-\Delta G_s$
C	50–75	73–85
Sn	30–35	61–87
P	32–41	76–80
Sb	8–25	83–130
S	50–58	165–190
H	65–68	71–109

of elements. Notice that carbon almost has a neutral effect whereas elements such as phosphorus, tin and antimony are notorious for their embrittlement potency.

It turns out that the values of these segregation energies can be estimated using electron theory. The difference $(\Delta G_b - \Delta G_s)$ for phosphorus has been confirmed using such calculations with a lower free energy for P in a free surface relative to a grain boundary.[28] The work has led to a greater insight into the mechanism of embrittlement. There is a costly structural rearrangement of the iron atoms in the grain boundary when P is introduced, which is partly responsible for the relatively small magnitude of ΔG_b. When molybdenum is added to the grain boundary, the embrittlement process is effectively reversed, not because it affects the embrittlement potency of phosphorus, but because it enhances cohesion at the grain boundary.

In similar theoretical work, Zhong *et al.*[29] showed that manganese on its own will embrittle iron, and further that Mn facilitates phosphorus embrittlement in the grain boundary by strengthening the in-plane P–Mn interaction, at the expense of cohesion across the boundary.

There are rumours that the same type of *ab initio* calculations indicate that the addition of small concentrations of palladium should reduce the tendency for embrittlement. There is some experimental evidence that the introduction of palladium into the surface of heat treated steel results in an elimination of hydrogen embrittlement.[30] It is fascinating that there are already attempts at designing martensitic creep-resistant steels based on Fe–Pd, steels which exploit the $L1_0$ FePd intermetallic compound for creep resistance.[31] On the basis of indications from electron theory, such alloys should show an enhanced resistance to embrittlement effects.

Avoiding Grain Boundary Embrittlement

The traditional routes for avoiding temper embrittlement involve a reduction in the impurity concentration and the addition of substitutional solutes which getter the impurities.[32]

A solute causes embrittlement by reducing the cohesion across the boundary plane. On the other hand, those solutes which enhance covalent bonding normal to the boundary must reduce embrittlement. *Ab initio* calculations of the bonding at grain boundaries in iron suggest this mechanism and confirm that phosphorus should embrittle and boron should toughen.[33]

Boron additions must therefore be useful in commercial, martensitic power plant steels, which can be made clean but not free of impurities. The difficulty, however, is that much of the boron enters the $M_{23}C_6$ phase[34] and hence less is available to segregate to the austenite grain boundaries. Much further work is needed on this topic.

Another possibility, which has never been investigated, would be to reduce the energy of the prior austenite grain boundaries. This could be done by making the austenite grain structure strongly crystallographically textured. The resulting austenite grain boundaries would have a high degree of fit and hence be less prone to impurity segregation. Whether this approach is worthwhile can in principle be predicted from *ab initio* calculations which can be attempted for a variety of different kinds of boundaries (albeit always at special orientations to minimise computations).

Summary: Electron Theory

Electron theory has not yet made a direct contribution to the design of creep-resistant steels. The potential is there if appropriate problems can be identified, for example, in the prediction of the stability of carbides and intermetallic compounds of the kind common in heat–resistant steels. Methods of reducing long-term embrittlement in multicomponent systems is another scenario where first principles calculations have been demonstrated to give valuable insight and qualitative guidance.

Table 4. Typical compositions (wt%) of creep-resistant steels. The range of alloys available is in fact much larger than this, for example, there is a variety of alloys available for bolting applications.

Designation	C	Si	Mn	Ni	Mo	Cr	V
1Cr$\frac{1}{2}$Mo	0.15	0.25	0.50	–	0.6	0.95	
$\frac{1}{4}$CrMoV	0.15	0.25	0.50	0.05	0.50	0.30	0.25
$\frac{1}{2}$Cr$\frac{1}{2}$Mo$\frac{1}{4}$V	0.12	0.25	0.50	–	0.6	0.45	0.25
1CrMoV	0.25	0.25	0.75	0.70	1.00	1.10	0.35
2$\frac{1}{4}$Cr1Mo	0.15	0.25	0.50	0.10	1.00	2.30	0.00
Mod. 2$\frac{1}{4}$Cr1Mo	0.1	0.05	0.5	0.16	1.00	2.30	0.25
						Ti=0.03	B=0.0024
2$\frac{1}{4}$Cr1.6WV	0.05	0.20	0.50	–	0.10	2.20	0.20
						W=1.60	Nb=0.05
3.0Cr1.5Mo	0.1	0.2	1.0	0.1	1.5	3.0	0.1
3.5NiCrMoV	0.24	0.01	0.20	3.50	0.45	1.70	0.10
9Cr1Mo	0.10	0.60	0.40	–	1.00	9.00	–
Mod. 9Cr1Mo	0.1	0.35	0.40	0.05	0.95	8.75	0.22
					Nb=0.08	N=0.05	Al <0.04
9Cr$\frac{1}{2}$MoWV	0.11	0.04	0.45	0.05	0.50	9.00	0.20
					W=1.84	Nb=0.07	N=0.05
12CrMoV	0.20	0.25	0.50	0.50	1.00	11.25	0.30
12CrMoVW	0.20	0.25	0.50	0.50	1.00	11.25	0.30
							W=0.35
12CrMoVNb	0.15	0.20	0.80	0.75	0.55	11.50	0.28
						Nb 0.30	N 0.06

7. The Steels

Some of the common heat-resistant steels are listed in **Table 4**. The leaner steels contain allotriomorphic ferrite and pearlite, but the majority have bainitic or martensitic microstructures in the normalised condition. Given the trend towards higher service temperatures, the trend in steel development has been towards higher chromium concentrations so the most modern of alloys occur towards the lower end of the table. A notable exception is the 2¼Cr1.6WV

alloy developed recently for boiler applications where post-weld heat treatment can be tedious and sometimes impractical.[35] It is a modification of the 2¼Cr1Mo alloy with the molybdenum substituted with tungsten; a reduction in the carbon concentration leads to a bainitic microstructure without martensite, allowing welding without pre- or post-weld heat treatment. The maximum hardness obtained for typical cooling rates is reduced to about 300 HV which is some 50 HV below that of 2¼Cr1Mo steel (**Fig. 5**). The insensitivity of the hardness to the cooling rate is claimed to be desirable in the design of joints.

8. Appearance, Disappearance and Reappearance of Carbides

Most steels are tempered severely prior to service in order to induce carbides or other precipitates and to relieve stresses. Some common precipitates are listed in Fig. 5(b); they determine the microstructure and are crucial in the development of creep strain. It is important to note that many of the precipitates are metastable in that they do not represent the lowest free energy state but nevertheless form because they can nucleate easily. They may therefore dissolve with time as the material approaches equilibrium. Sometimes, carbides which are metastable at first, become stable during service when the composition of the steel changes. This happens when two different kinds of steels are joined together, leading to diffusion fluxes across the junction.[36] **Figure 6**(a) shows a case where the carbon concentration of a 2¼Cr1Mo which is joined to a mild steel increases during the course of service because the carbon can sit more comfortably in the chromium-containing steel than in the mild steel. The material at first contains just $M_{23}C_6$ and M_7C_3; the latter dissolves but reappears as the carbon concentration rises to 0.28 wt%. Furthermore, metastable cementite which is always present at the earliest stages of tempering, reappears as the equilibrium phase when the carbon concentration rises to 0.56 wt%. The task is to model the evolution of precipitation, dissolution and coarsening reactions.

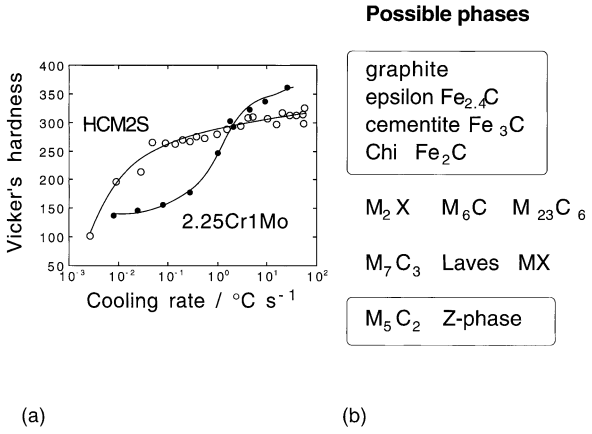

Fig. 5. (a) A comparison between the hardness of a tungsten strengthened creep resistant steel and the classical 2¼Cr1Mo alloy. The cooling rate is an average value in the range 800–300°C s^{-1}. Data from Komai *et al.*[35] (b) The precipitate phases in power plant steels. The iron-rich carbides such as cementite form rapidly, whereas graphite, although an equilibrium phase, is difficult to nucleate.

The results of equilibrium calculations which give the phase fractions of the carbides as a function of the overall alloy composition and temperature, are given in Fig. 6(b) for the common power plant steels. The calculations have been done using the MTDATA[37] computer program and SGTE database, taking into account the carbide phases and Laves phase listed, together with cementite. The chemical elements considered are carbon, silicon, manganese, chromium, nickel, molybdenum, vanadium, niobium and nitrogen. M_5C_2 has recently been identified in 1Cr–0.5Mo steels[38] but along with graphite, has not been included in the analysis.

Equilibrium calculations such as those presented in Fig. 6 are useful in specifying the ultimate microstructure but the results are far from the actual microstructures that exist during service. It is necessary in practice to be able to calculate time–temperature-transformation diagrams for tempering reactions, as a function of steel chemical composition and tempering temperature. In order to do this, a theory capable of handling several simultaneous precipitation reactions has been developed,[39,40] where the different phases influence each other, for example by drawing the same solute from the matrix ferrite.

9. First Order Reactions

Kelvin demonstrated in 1871 that without fluctuations it is impossible for a tiny droplet of water to condense from supersaturated vapour. The work needed to create the boundary between the droplet and vapour is, for a tiny droplet, prohibitive even for a supersaturated vapour. This is why the droplet has to form as a chance event and it may succeed in growing if its size is beyond critical. All precipitates in steels must nucleate in this same way, and hence are

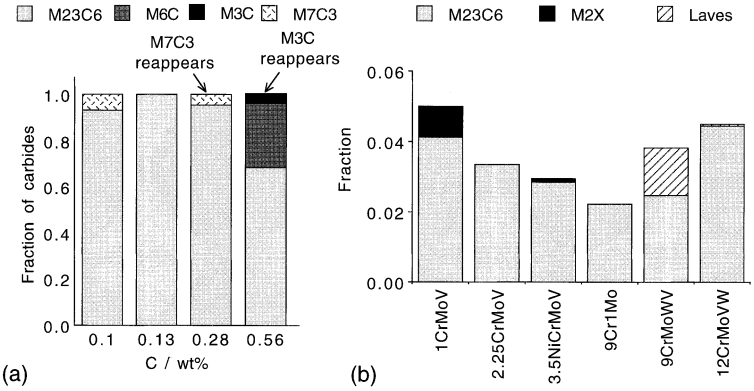

Fig. 6. (a) The equilibrium carbides in a 2¼Cr1Mo steel as a function of the carbon concentration.[36] (b) Equilibrium fractions of carbides in some common power plant steels, as calculated using MTDATA and the SGTE thermodynamic database for 565°C (838 K). Very small fractions of vanadium and niobium carbonitrides are are present in some steels but are not shown. Thus, the modified 9Cr1Mo contains 0.0009 NbN and 0.003 VN, the 9CrMoWV steel contains 0.0008 NbN and 0.0032 VN. The calculations allowed the existence of all the carbides described in Fig. 5 with the exception of graphite, epsilon, Chi, Z-phase and M_5C_2.

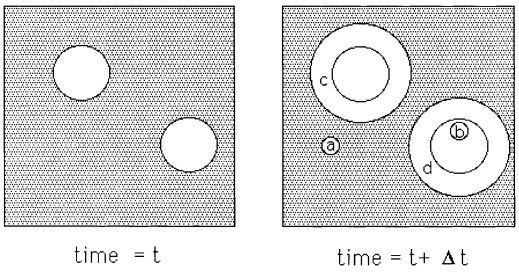

Fig. 7. The concept of extended volume. Two precipitate particles have nucleated and grown to a finite size in the time *t*. New regions c and d are formed as the original particles grow, but a and b are new particles, of which b is unreal because it has formed in a region which is already transformed.

called first order reactions in the Ehrenfest classification. Growth is defined beyond the critical nucleus size. Nucleation and growth are well known phenomena but to calculate volume fraction requires a treatment of the impingement between particles growing from different sites. This is generally done using the extended volume concept of Johnson, Mehl, Avrami, and Kolmogorov[41] as illustrated in **Fig. 7**. Suppose that two particles exist at time *t*; a small interval δt later, new regions marked a, b, c and d are formed assuming that they are able to grow unrestricted in extended space whether or not the region into which they grow is already transformed. However, only those components of a, b, c and d which lie in previously untransformed matrix can contribute to a change in the real volume of the product phase (identified by the subscript '1') so that:

$$dV_1 = \left(1 - \frac{V_1}{V}\right) dV_1^{\mathrm{e}} \quad \text{.....(1)}$$

where it is assumed that the microstructure develops randomly. The superscript e refers to extended volume, V_1 is the volume of phase 1 and V is the total volume. Multiplying the change in extended volume by the probability of finding untransformed regions has the effect of excluding regions such as b, which clearly cannot contribute to the real change in volume of the product. The extended volume term is of course easy to calculate from the nucleation and growth rates, because it neglects impingement but it is the real volume that is needed. This requires the equation to be integrated to obtain the real volume fraction,

$$\frac{V_1}{V} = 1 - \exp\left\{-\frac{V_1^{\mathrm{e}}}{V}\right\} \quad \text{.....(2)}$$

10. Many Reactions Occurring Together

Many of the precipitates found in power plant steels (Fig. 5(b)) have crystal structures and compositions which are quite different from those of the ferrite matrix. The precipitate/matrix interfacial energy can therefore be expected to be large, making it difficult for the equilibrium precipitate to nucleate. Consequently, decomposition often starts with the formation of one or more metastable phases which are kinetically favoured. These must eventually dissolve as equilibrium is approached. It follows that many precipitation and dissolution reactions may occur simultaneously. Of course, it does not require metastability to cause the formation of more than one precipitate phase. All power plant steels have many components so the final equilibrium state may contain many phases, as is evident in Fig. 6.

Table 5. Concentration (in wt%) of the major alloying elements in the steels used to demonstrate the model.

	C	N	Mn	Cr	Mo	Ni	V	Nb
$2\frac{1}{4}$Cr1Mo	0.15	–	0.50	2.12	0.9	0.17	–	–
3Cr1.5Mo	0.1	–	1.0	3.0	1.5	0.1	0.1	–
10CrMoV	0.11	0.056	0.50	10.22	1.42	0.55	0.20	0.50

When more than one reaction occurs at the same time, they interfere with each other in a way which is seminal to the development of power plant microstructures. It is not possible to deal with more than one reaction at time using ordinary Avrami theory, but a recent adaptation has generalised the theory for simultaneous reactions.[39,40] When phases β and θ precipitate at the same time from a parent phase α Eq. (2) is replaced by a pair of coupled equations as follows:

$$dV_\beta = \left(1 - \frac{V_\beta + V_\theta}{V}\right) dV_\beta^{\mathrm{e}} \quad \text{.....(3)}$$

and similarly for θ,

$$dV_\theta = \left(1 - \frac{V_\beta + V_\theta}{V}\right) dV_\theta^{\mathrm{e}} \quad \text{.....(4)}$$

Since V_β is in general expected to be some complicated function of V_θ, numerical integration is used and exploited to change the boundary conditions for nucleation and growth during the course of transformation, thus accounting for the change in the matrix composition using a mean field approximation. The method can in principle be applied to any number of simultaneous reactions with a corresponding set of coupled equations.

11. Time–Temperature Precipitation Diagrams

The compositions of three power plant alloys used here for illustration purposes, are shown in **Table 5**. These three alloys, whilst of quite different chemical compositions, show similar precipitation sequences[39,42,43] but with vastly different rates. For example, at 600°C the time taken before $M_{23}C_6$ is observed is 1 h in the 10CrMoV steel,[39] 10 h in the 3Cr1.5Mo alloy[42] and in excess of 1 000 h in the 2¼Cr1Mo steel.[43] These differences were not explained prior to the simultaneous transformations model.[39]

A plot of the volume fraction of each precipitate as a function of time at 600 °C is shown in **Fig. 8**. Consistent with experiments, the precipitation kinetics of $M_{23}C_6$ are predicted to be much slower in the 2¼Cr1Mo steel compared to the 10CrMoV and 3Cr1.5Mo alloys. One contributing factor is that in the 2¼Cr1Mo steel a relatively large volume fraction of M_2X and M_7C_3 form prior to $M_{23}C_6$. These deplete the matrix and therefore suppress $M_{23}C_6$ precipitation. The volume fraction of M_2X which forms in the 10CrMoV steel is relatively small, and there remains a considerable excess of solute in the matrix, al-

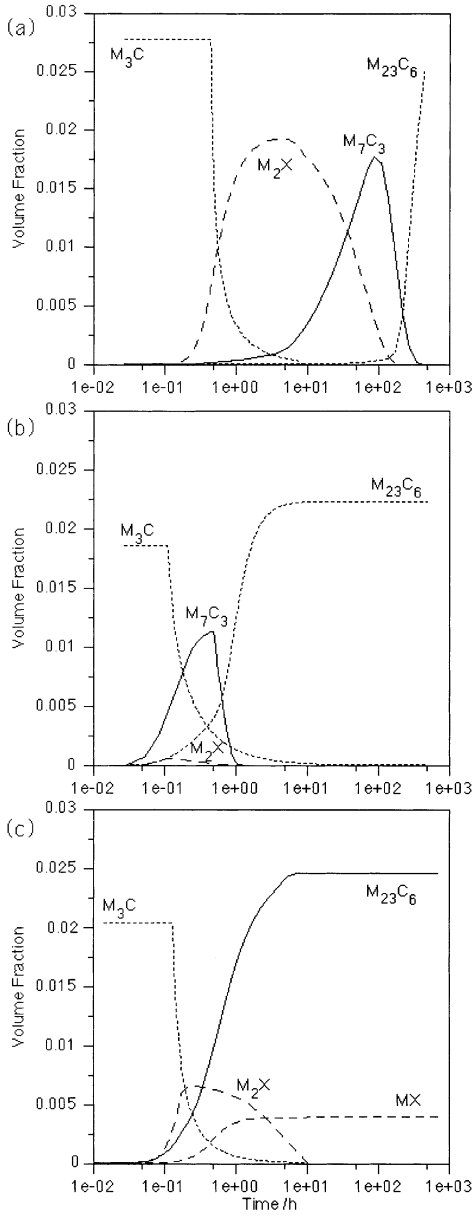

Fig. 8. The predicted evolution of precipitate volume fractions at 600°C for three power plant materials (a) 2¼Cr1Mo, (b) 3Cr1.5Mo and (c) 10CrMoV.[39]

lowing $M_{23}C_6$ to precipitate rapidly. Similarly, in the 3Cr1.5Mo steel the volume fractions of M_2X and M_7C_3 are insufficient to suppress $M_{23}C_6$ precipitation to the same extent as in the 2¼Cr1Mo steel.

$M_{23}C_6$ is frequently observed in the form of coarse particles which are less effective in hindering creep deformation. Delaying its precipitation would have the effect of stabilising the finer dispersions of M_2X and MX to longer times with a possible enhancement of creep strength. Calculations like these have been used to design the microstructures of novel steels[17] and their application has been extended to other areas including for example, the microalloyed structural steels.[44]

12. Stability of the Microstructure

Consider a particulate phase θ in a ferritic matrix α. The solute concentration in the ferrite is written $c^{\alpha\theta}$ and that in

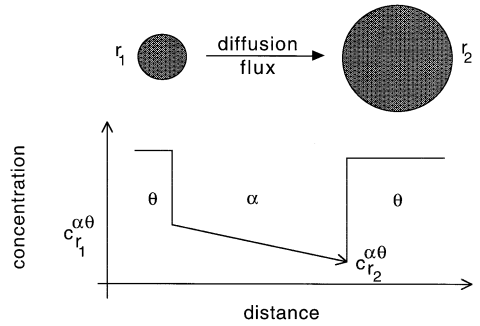

Fig. 9. An illustration of the capillarity effect driving coarsening.

θ written $c^{\theta\alpha}$ assuming that the two phases are in equilibrium at a flat interface. However, if the interface is curved, for example when the particles are in the form of spheres, the equilibrium concentrations become a function of the radius of curvature, given by $c_r^{\alpha\theta}$ and $c_r^{\theta\alpha}$ respectively, where r is the particle radius. This is the Gibbs–Thompson capillarity effect. It accounts for the cost of creating interface as the particle grows.

It can be shown that the concentration $c_r^{\alpha\theta} > c^{\alpha\theta}$, the inequality becoming larger as $r \to 0$. In other words, the solute concentration in the ferrite near a small particle will be greater than that in contact with a large particle, thus setting up a concentration gradient which makes the small particle dissolve and the larger particle grow (**Fig. 9**). This is the process of coarsening, driven by the interfacial energy σ.

The concentration difference $c_r^{\alpha\theta} - c^{\alpha\theta}$ which drives the diffusion flux is given by:

$$c_r^{\alpha\theta} - c^{\alpha\theta} = \frac{\sigma V^{\alpha}}{kTr} \times \frac{c^{\alpha\theta}(1-c^{\alpha\theta})}{c^{\theta\alpha} - c^{\alpha\theta}} \quad \text{.....(5)}$$

where k is the Boltzmann constant, T the absolute temperature and V^{α} the molar volume of the ferrite. This flux feeds the growth or dissolution of the particle and hence must match the rate at which solute is absorbed or desorbed at the moving interface:

$$\underbrace{D(c_r^{\alpha\theta} - c^{\alpha\theta})}_{\text{measure of flux}} \quad \propto \quad \underbrace{v(c^{\theta\alpha} - c^{\alpha\theta})}_{\text{rate of solute absorption}}$$

where v is the interfacial velocity and D is the solute diffusivity in the matrix phase. On substituting for the concentration difference and using Fick's first law, it follows that:

$$v \propto D \frac{\sigma V^{\alpha}}{kTr} \times \underbrace{\frac{c^{\alpha\theta}(1-c^{\alpha\theta})}{(c^{\theta\alpha} - c^{\alpha\theta})^2}}_{\text{instability}} \quad \text{.....(6)}$$

In Eq. (6), the equilibrium concentration term on the right is a thermodynamic term, a larger value of which corresponds to a greater coarsening rate. For a large variety of power plant steels, **Fig. 10** shows the equilibrium chromium concentrations in the ferrite and $M_{23}C_6$ phases. The concentrations are clearly largest for the more modern martensitic alloys which are Cr-rich; such steels are designed for higher temperature service and hence require a greater oxidation resistance. It is also evident, however, that the tendency for $M_{23}C_6$ to coarsen should also be greatest in the Cr-rich al-

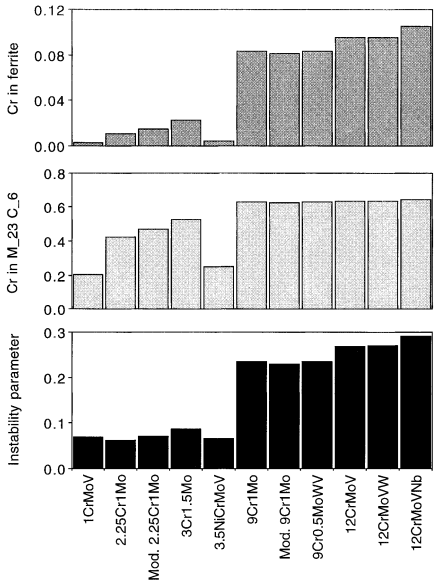

Fig. 10. The top two bar charts give the chromium concentrations (mole fractions) in ferrite and in $M_{23}C_6$ respectively. The actual compositions of the steels are given in Ref. 45). The third bar chart is gives a measure of the tendency for $M_{23}C_6$ to coarsen assuming Eq. (6).

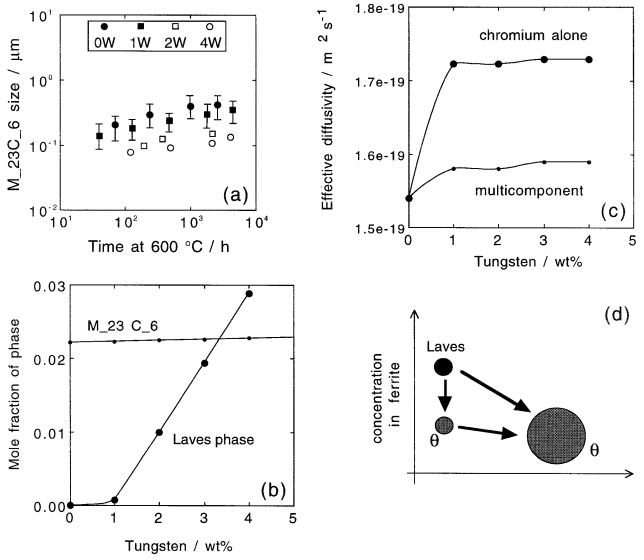

Fig. 11. Coarsening data from Fe–0.1C–9Cr–0.5Mn–0.3Siwt% steel, containing a variety of tungsten additions, tested in creep at 600°C [Abe]. (a) $M_{23}C_6$ size. The error bars have been omitted for the highest W data for clarity. (b) Equilibrium phase fraction calculations for 600°C carried out using MTDATA with the SGTE database, allowing all common carbides and Laves phase and Fe, C, Cr, Mn, Si, W as the components. (c) Values of D_{eff} for $M_{23}C_6$, for two cases, the first where chromium alone is considered and then for multicomponent diffusion. (d) Schematic illustration of why the presence of Laves phase retards the coarsening of $M_{23}C_6$.

loys.

Commercial steels contain many solutes whereas Eq. (6) deals with just one. Venugopalan and Kirkaldy[46] generalised the theory to deal with many solutes, assuming that the effects of the different fluxes could be combined into a single, effective diffusion coefficient D_{eff} by treating the fluxes as a combination of parallel electrical conductances. Equation (6) can be rearranged as follows:

$$\frac{1}{v} \propto \frac{1}{D_i} \times \frac{(c_i^{\theta\alpha} - c_i^{\alpha\theta})^2}{c_i^{\alpha\theta}(1 - c_i^{\alpha\theta})} \quad \text{.....(6)}$$

where i now represents a particular solute. In a multicomponent alloy, the right hand side is replaced by a summation.

$$\frac{1}{v} \propto \frac{1}{D_{\text{eff}}} \quad \text{where} \quad \frac{1}{D_{\text{eff}}} = \sum_i \frac{1}{D_i} \times \frac{(c_i^{\theta\alpha} - c_i^{\alpha\theta})^2}{c_i^{\alpha\theta}(1 - c_i^{\alpha\theta})} \quad \text{.....(7)}$$

This multicomponent treatment does not in fact make a difference to the ranking of the $M_{23}C_6$ coarsening tendency as presented in Fig. 10, because this carbide is chromium-rich and because the diffusivities of the substitutional solutes are not very different.

Coarsening in Multiphase Microstructures

Abe[47] has reported interesting data on the coarsening of $M_{23}C_6$ particles in Fe–9Cr–W steels as a function of the tungsten content and of time during creep testing at 600 °C (**Fig. 11**(a)). According to Abe, the addition of tungsten reduces the coarsening rate. The data have to be interpreted with care because the addition of tungsten also causes the precipitation of Laves phase (Fig. 11(b)), but the fact that the data are from creep test samples should not matter since it is the trend as a function of W that we are interested in; we shall also assume that the electron microscopy data refer strictly to $M_{23}C_6$ and do not unintentionally include any other phases. Figure 11(c) shows two sets of calculated values of D_{eff}, one assuming that it is only the diffusion of chromium (the major constituent of $M_{23}C_6$ in such alloys) that controls coarsening, and the other using the multicomponent formalism (Eq. (7)). As stated earlier, the trends are identical for the two sets of calculations, but in contradiction to the experimental data, they all suggest that the addition of tungsten should accelerate the rate at which $M_{23}C_6$ coarsens. The calculations show also that the experimental data cannot be explained by saying that tungsten reduces the overall diffusion coefficient.[47]

A possible explanation is that Laves phase precipitates some time after $M_{23}C_6$, in which case it may be appropriate to consider a constrained equilibrium in which Laves phase is excluded. In fact, when this is done, M_6C is promoted and the situation worsens in the sense that D_{eff} for $M_{23}C_6$ is predicted to increase.

The problem of explaining why the addition of tungsten reduces the coarsening of $M_{23}C_6$ can be explained by taking into account all of the phases that are present. When there is more than one precipitate phase in the microstructure, differences in interfacial energy (σ, Eq. (7)) cannot be neglected. Laves phase has a higher interfacial energy so the concentration in ferrite in equilibrium with Laves will, for the same particle radius, be higher for Laves than for $M_{23}C_6$:

$$c^{\alpha\theta}_{r,\,\text{Laves}} > c^{\alpha\theta}_{r,\,M_{23}C_6}$$

This is illustrated schematically in Fig. 11(d) on a concentration–distance plot. In addition to a flux of solute from

small Laves phase particles to larger ones, there will also be a flux to both small and large $M_{23}C_6$ particles. The coarsening rate of $M_{23}C_6$ will therefore be reduced whereas that of Laves phase accelerated. It is interesting that Abe specifically commented that the coarsening rate of Laves phase was extremely rapid.

Proper calculations of coarsening in multiphase systems will become possible in the near future, most likely within the framework of the simultaneous transformations model discussed earlier. In that case, the coarsening kinetics do not require an explicit treatment but follow naturally from the precipitation theory which for each phase includes the capillarity effect. Indeed, it is well know that the separation of precipitation and coarsening is artificial, because capillarity makes the smaller precipitates grow at a slower rate than those which nucleated first and hence are larger, even before the equilibrium fraction is reached.[44] **Figure 12** shows the results of calculations of this kind, the mean particle radius at first increasing approximately parabolically with time as all particles grow from solid solution. The mean radius then changes as about $t^{1/3}$ at longer times as the number density of particles decreases, consistent with expectations from coarsening theory. It is important to emphasise that there is no separate treatment of precipitation and coarsening here, both are in an inclusive theory.

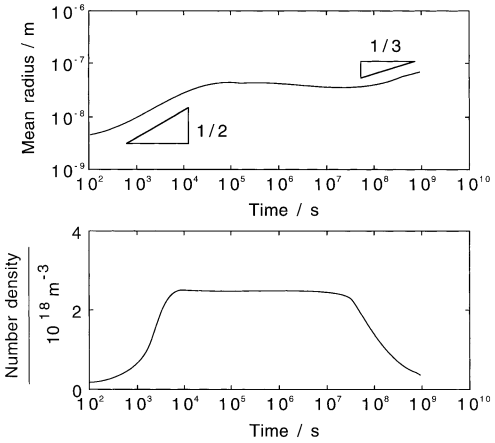

Fig. 12. The precipitation and coarsening of niobium carbide precipitates in austenite[44] in Fe–0.05Nb–0.1C wt% steel, beginning with a supersaturated solid solution at 900 °C. The number density of nucleation sites was taken to be $9\times10^{19}\,m^{-3}$, with $\theta=0.26\,J\,m^{-2}$.[44]

13. The Matrix Microstructure

The most exciting ferritic creep-resistant steels start with a microstructure which is martensitic.[5,48] On the other hand, the best established steels of this kind rely on allotriomorphic ferrite or bainite as the starting microstructure. Why are modern heat-resistant steels based on martensite? Is the martensite desirable and can it be altered to better fit the purpose?[49] And how do calculations contribute to this exercise?

Low-chromium steels, such as the classical 2¼Cr1Mo or 1CrMoV alloys have formed the backbone of the power generation and petrochemical industries for at least five decades, for operating temperatures of 565°C or less. The 2¼Cr1Mo is essentially bainitic, whereas the 9Cr1Mo type alloys developed much later, for higher temperatures and greater corrosion/oxidation resistance, are martensitic. **Figure 13**(a) shows that in the unmodified form the 9Cr1Mo does not have a superior creep rupture performance.

The answer must be that the martensitic matrix arises by chance. The chromium concentration was increased for oxidation and corrosion resistance with balancing additions of other solutes to avoid δ-ferrite. The hardenability then becomes sufficiently large to induce martensite instead of bainite for identical cooling conditions. This is illustrated by the calculated[50] time–temperature transformation diagrams for 2.3, 4.3, and 9.3 wt% chromium steels in Fig. 13(b).

Martensite, Bainite and Precipitation

Could it be that the martensitic microstructure, which has a very high number density of defects, encourages the precipitation of more numerous and finer carbide particles which resist creep deformation? Baker and Nutting[24] conducted a transmission electron microscope study of carbide precipitation reactions during the isothermal tempering of a 2¼Cr1Mo steel in two starting microstructural conditions, bainite and martensite. Whereas the kinetics of precipitation were not found to be exactly identical in the two cases, the differences were small over the temperature range of interest (500–650°C). In hindsight this might be expected since both microstructures contain similar defect densities (dislocations, plate boundaries, austenite grain boundaries); the slightly smaller defect density expected in bainite does not seem to have any significant effect on the precipitation kinetics. A bainitic microstructure should therefore be ade-

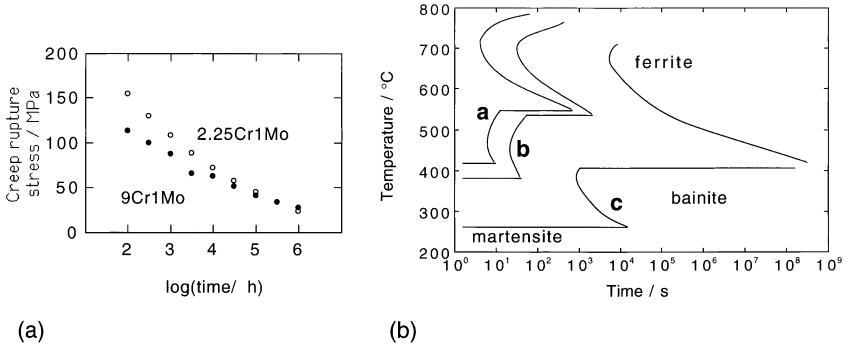

Fig. 13. (a, b) Calculated rupture strength as a function of time for a bainitic (low Cr) and martensitic (high Cr) steel. The exact compositions are 0.15C–0.25Si–0.50Mn–2.3Cr–1Mo–0.10Niwt% and 0.10C–0.60Si–0.40Mn–9.0Cr–1Mo–0.00Niwt% following an identical heat treatment consisting of 1 056°C for 12 h, 740°C for 13 h. The details can be found in Refs. 17),51). (c) Calculated[50] time–temperature transformation diagrams for steels **x** (0.15C–0.25Si–0.5Mn–1Mo–2.3Cr wt%), **y** (4.3Cr) and **z** (9.3Cr). The transformation curves refer to zero percent reaction. In each case the upper curve represents diffusional transformation whereas the lower curve represents bainite.

quate and martensitic steels have the additional burden that they are difficult to weld.

Plate Boundaries

Extremely fine dispersions of carbides can be achieved in microstructures other than martensite. For example, during the transformation of ferrite to austenite. "Interphase precipitation" is a term used to describe the precipitation of a third phase at the α/γ interface during the transformation of austenite to ferrite.[52] Ferrite grains are obtained which are tens of microns containing the fine dispersions of precipitates. These microstructures are not the most popular in heat-resistant steels, presumably because the plate boundaries of martensite or bainite are themselves an impediment to dislocation motion. When the mechanism of creep is one controlled by the climb of dislocations over precipitates, there must be an advantage to refining the matrix plate size. What controls the size of the martensite or bainite plates?

This steels of the type considered here, the enormous shear-dominant shape deformation accompanying martensitic or bainitic transformation is not elastically accommodated. The dislocation debris generated as the transformation strain is plastically accommodated resists the advance of the bainite/austenite interface, the resistance being greatest with strong austenite. The strength of austenite must therefore feature in any assessment of plate size; indeed, this effect has been known for some time.[53,54] The plates are expected to become thicker at high temperatures, where the austenite has a lower yield strength. Dynamic recovery at high temperatures should further weaken the austenite and lead to coarser plates.

The thickness must also be influenced by impingement between adjacent plates; a large nucleation rate must naturally refine the microstructure.

The observed effect of temperature could easily be indirect since both the austenite strength and the nucleation rates are strongly dependent on temperature and the composition of the steel. A quantitative analysis of the bainite plate thickness as a function of the strength of the austenite, the chemical free energy change accompanying transformation and the transformation temperature has shown that the latter has only a small independent effect on the thickness (**Fig. 14**). Strong austenite and high driving forces lead to a finer microstructure.

Controlled experiments are now needed to discover whether the creep resistance of steels increases as the plate thickness is reduced. Obviously, any refinement of the microstructure should not be so large that the mechanism of creep changes, from one controlled by the climb of dislocations over obstacles, to one dominated by diffusion along martensite boundaries. However, this is unlikely to be an issue because the boundaries between martensite plates in a given austenite grain tend to have a high degree of coherence.

To summarise, there is probably an advantage in maintaining the martensite plate size as fine as possible. In the context of heat-resistant steels, this can be done by strengthening the austenite, particularly solid-solution strengthening.

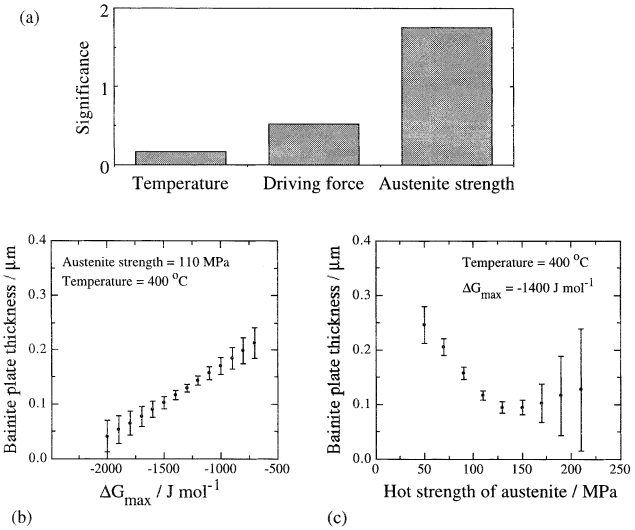

Fig. 14. (a) The model perceived significance of each of the variables plotted on the horizontal axis, in influencing the thickness of bainite plates. The vertical scale represents the ability of the variable to explain variations in plate thickness. (b) Variation in thickness with the chemical driving force. (c) Variation in thickness with the strength of the austenite. After Singh and Bhadeshia.[55]

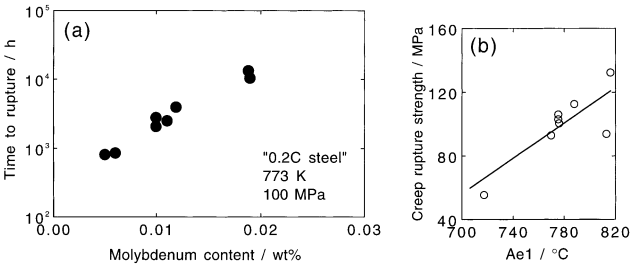

Fig. 15. (a) The effect of frequently ignored trace concentrations of molybdenum on the creep strength of steel [Kimura]. (b) Correlation of the measured 100 000 h creep rupture strength of different alloys tested at 600°C against the equilibrium Ae_1 temperature.[7]

14. Mechanical Properties: The Enigma

A reasonable view is that we know and understand a great deal about mechanical properties, but that a quantitative treatment in terms of the parameters important in alloy design is in the distant future. We are forced therefore to make design decisions based on inductive rather than deductive thinking. Most of the research on microstructure–property relationships begins with a reduction of variables. This simplifies experiments but there is a penalty that the work is far removed from technology.

Parameters which are known to influence properties are sometimes neglected in experiments and their analysis. This has at least two effects. The first is that it introduces "noise" in the predictions, *i.e.* scatter. This was demonstrated for creep-resistant steels recently by Kimura *et al.*[48] who found that an enormous scatter in the creep rupture life of a particular alloy could be eliminated by taking into account residual concentrations of molybdenum (**Fig. 15**(a)).

The second important effect of neglected variables is that analysis of the results can lead to an incorrect inference. This might seem obvious since predictions are more noisy when all influences are not taken into account. This can be

Table 6. Coefficients for an equation of the form $y=\sum_i w_i x_i+\theta$ where y is the dependent variable, x_i are the independent variables; w_i are the regression coefficients, θ is the regression constant and r is the correlation coefficient. The first column gives the variables that were taken into account in deriving the regression parameters.

Variables	w_1	w_2	θ	r
x_1 and x_2	0.879	0.086	-1.913	0.739
x_1	1.036		-2.359	0.706
x_2		0.244	5.060	0.400

illustrated quantitatively using linear regression analysis. **Table 6** shows that the coefficients from multiple regression analysis are different from those when relevant variables are excluded. Recent publications have emphasised that a high Ac_1 temperature (where austenite formation first begins during heating) leads to good creep strength (Fig. 15 (b)).[7,14,15] However, a plot of the creep strength of a variety of steels *versus* a single variable, such as the Ae_1 temperature, may not reveal a true effect of the transformation temperature. Indeed, there does not seem to be a mechanism for the proposed effect.

Neural Networks

There are no obvious physical models capable of estimating anything but the simplest of mechanical properties, certainly nothing as far as the creep rupture stress is concerned. Linear regression is too limited in its form. A neural network is capable of realising a greater variety of non-linear relationships of considerable complexity. Data are presented to the network in the form of input and output parameters, and the optimum non-linear relationship is found by minimising a penalised likelihood. The results consist of a specification of the function, which in combination with a series of coefficients (called weights), relates the inputs to the outputs. The search for the optimum representation can be computer intensive, but once the process is completed (*i.e.* the network trained) the estimation of the outputs is very rapid.

Introductory papers on the neural network method, particularly in the context of materials science, can be found elsewhere.[56,57] Suffice it to say that in this nonlinear method it is possible to control overfitting; to take account of any level of interactions between the variables; to make predictions which have two components in the error bars—one representing the perceived level of noise in the output and the second[56,58] indicating the uncertainty of fitting the data. This second component, which comes from a Bayesian framework, allows the relative probabilities of models of different complexity to be assessed and hence to obtain quantitative error bars which vary with the position in input space, depending on the uncertainty of fitting the function in that region of space. In the opinion of the author, this methodology has had a liberating effect on materials science in that we are now able to model the most complex of mechanical properties whilst at the same time revealing new patterns of behaviour and making use of the predictions in alloy design.[57] We now proceed to describe neural network models on creep rupture strength.

Table 7. The standard set of input parameters in a neural network model of creep rupture strength.[17,51] The chemical compositions are all in wt%.

STEEL	$2\frac{1}{4}$CrMo	10CrMoW
Normalising temperature / K	1203	1338
Duration / h	6	2
Cooling rate	water quenched	air cooled
Tempering temperature / K	908	1043
Duration / h	6	4
Cooling rate	air cooled	air cooled
Annealing temperature / K	873	1013
Duration / h	2	4
Cooling rate	air cooled	air cooled
C wt%	0.15	0.12
Si	0.21	0.05
Mn	0.53	0.64
P	0.012	0.016
S	0.012	0.001
Cr	2.4	10.61
Mo	1.01	0.44
W	0.01	1.87
Ni	0.14	0.32
Cu	0.16	0.86
V	0.01	0.21
Nb	0.005	0.01
N	0.0108	0.064
Al	0.018	0.022
B	0.0003	0.0022
Co	0.05	0.015
Ta	0.0003	0.0003
O	0.01	0.01
Re	0.00	0.00

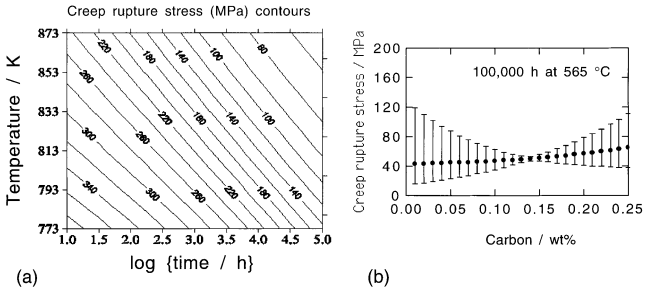

Fig. 16. (a) Contour plot of the calculated creep rupture strength as a function of the temperature and time, for the 2¼Cr1Mo steel listed in Table 7. The error bar on each stress is only about ±10 % of the quoted value. (b) The calculated creep rupture strength at 565 °C, 100 000 h for the same 2¼Cr1Mo steel but as a function of the carbon concentration.

15. Estimation of Creep Rupture Strength

An experimental dataset is essential in neural network analysis. **Table 7** illustrates for two typical alloys, a set of 37 variables used in the compilation of creep data for neural network analysis (note that the cooling rate counts as up to four separate variables). In fact, it is not difficult to imagine an even larger list of variables which could influence creep, but an over ambitious choice of inputs is likely to reduce the number of data available in the literature. However, the full chemical composition and heat treatment is clearly the minimum information necessary since the microstructure depends critically on these variables. We believe that Table

7 represents the minimum number of variables that must be specified and reported in any future experimental measurement.

Figure 16(a) shows some typical calculations possible with the model, for the 2¼Cr1Mo steel listed in Table 7. Notice that the region in which there is the sharpest decline in the creep strength with time, *i.e.* the shortest spacing between the contours, appears at shorter times as the temperature is increased. This is to be expected since coarsening reactions are accelerated at high temperatures and once coarsening becomes significant, the contours again become widely spaced as the inherent strength[48] of the matrix is reached, in this case about 40–80 MPa.

Figure 16(b) illustrates two important points. First, the error bars are clearly a function of the carbon concentration and indicate that there is insufficient knowledge about the creep properties of 2¼Cr1Mo steel for the specified set of parameters, when the carbon concentration falls outside the range 0.1–0.2 wt%. This is useful because large error bars indicate that new experiments are necessary before the prediction can be taken to heart. The second consideration is that the commercial specification of 2¼Cr1Mo steel only states a maximum carbon concentration of 0.16 wt%, there is no minimum.[59] This clearly is unsatisfactory.

Calculations like these can now be carried out routinely and the associated software is available freely on the world wide web.*2 Furthermore, the models can be improved both as more data become available and as creep deformation becomes better understood. The model can be used in a variety of ways. The combined application of the physical models presented earlier, and the neural network model has led to predictions of novel alloys which ought to have much better creep resistance than any comparable commercial alloy.[17,51] There are long-term experiments in progress to test these designer-alloys. Another way is to apply the models to welding alloys, for which there are much fewer data when compared with wrought steels.

16. Welding Alloys

It has been argued that weld metals and steels of matching composition seem to have similar creep rupture properties.[51,60] Weld metal is expected to have a higher oxygen and nitrogen concentration but the former should not affect creep resistance. Although differences in the nitrogen concentration are important, they can be taken into account both in predicting carbonitride formation and in the neural network model where nitrogen is an input.

The microstructure of an as-deposited weld metal is naturally radically different from that of a wrought steel. However, even this is unimportant because the severe tempering heat treatments used following the welding procedure, essentially wipe out the original microstructure and replace it with one which is tempered and similar to that of the steel plate.

Cole *et al.*[51,60] have developed a procedure in which the model for the creep rupture life of wrought steels can be used to estimate the properties of weld metals, by giving a notional austenitisation heat treatment to the weld even though such a treatment is absent in real life. **Figure 17** shows the very encouraging agreement between the predicted and measured[61] creep rupture lives of alloys designed for the welding of NF616, even to times up to 40 000 h at temperature. The predictions are made without any adjustment of the models, which did not interrogate any weld metal data during their creation. The results confirm that it is reasonable to assume that weld metal creep rupture life can be modelled on the basis of wrought steels.

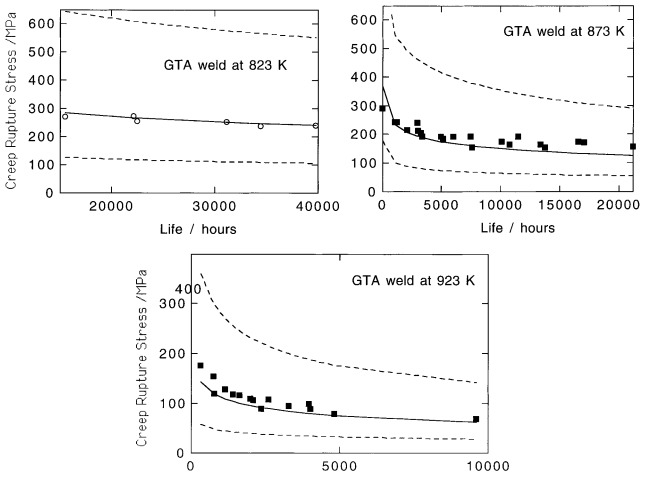

Fig. 17. The impressive agreement between the calculated[51] and measured[61] creep rupture stresses for NF616 type welding alloys.

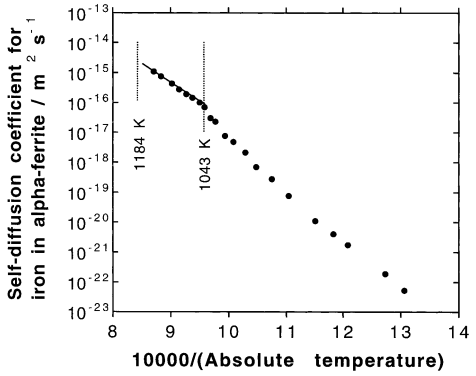

Fig. 18. Self-diffusion coefficient of iron in α-ferrite.[65] The Curie temperature is 1 043 K and the formation of austenite begins at 1 184 K.

17. Self-diffusion in Iron

The way in which solutes affect the diffusivity of iron atoms can now be calculated using commercially available software and databases,[8] although exploitation of the results in creep design has yet to be established. A detailed discussion can be found elsewhere[62] but it is worth emphasising that magnetism has a large role to play. Self-diffusion data for ferrite show anomalies, both in the region of paramagnetic to ferromagnetic transition and in the δ-ferrite temperature range **Fig. 18**.[63–65] The anomaly has been observed also for the diffusion of nickel in ferrite[66] and in a vast range of other measurements including mechanical properties such as creep at elevated temperatures.

*2 www.msm.cam.ac.uk/map/mapmain.htm

To cut a long story[62] short, Kučera[67] proposed a function of the form to explain diffusion in ferrite:

$$D = D_0 \exp\left\{\frac{0.35q\{T\}Q_0}{RT_m}\right\}\exp\left\{-\frac{Q}{RT}\right\} \quad \text{.....(8)}$$

and Jönsson[68] expressed the function q in terms of thermodynamic parameters alone,

$$q\{T\} = b_3^{mg}\Delta H\{T\}$$

where b_3 is a fitting constant and ${}^{mg}\Delta H\{T\}$ is the excess magnetic enthalpy at the temperature T. Equation (8) contains the melting temperature whose meaning in the context of diffusion is not clear for an alloy where melting occurs over a range of temperatures. However, there is a well known empirical relationship between the activation energy for diffusion and the melting temperature of a pure metal,

$$Q_0 = 140T_m \quad (\text{J mol}^{-1})$$

so that the melting temperature can be eliminated from Eq. (8). By fitting the equation to ferritic iron, Jönsson was able to demonstrate that with appropriate thermodynamic data for ${}^{mg}\Delta H$, he was able to estimate fairly well the tracer diffusion of elements such as cobalt, nickel in ferrite both in the ferromagnetic and paramagnetic regions. The activation energy and D_o for the paramagnetic state derived by fitting in each case but b_3 was kept fixed, assumed to depend only on the lattice geometry.

To summarise, it is possible, when the thermodynamic data necessary for the estimation of ${}^{mg}\Delta H\{T\}$ are available, to calculate the effect of solute elements on the tracer diffusion coefficient of iron. It will be interesting to see how such information can be exploited in the design of creep-resistant steels.

18. Summary

In spite of uncertainties and many remaining problems, it is now possible to attempt a quantitative design of heat resistant steels and welding alloys. This is true both with respect to the energetics and kinetics of microstructural evolution and in the estimation of creep rupture life.

It will be necessary in the longer term for the microstructure models to predict particle size and spatial distributions, and to account for the effect of stress and strain on transformation kinetics. It is likely that mechanical property models which use a large number of variables will be the only ones that succeed in bridging the gap between microstructure and complex properties.

Whatever happens, the development of creep resistant steels probably represents and will continue to be the most exciting and fruitful research and development exercise in all of materials science. And this applies to both industry and academia, who are working together without the need for imposed stimuli from government or well–meaning analysts of educational and commercial philosophy!

Acknowledgments

I am grateful to the organisers of Parsons 2000 for the opportunity of presenting this lecture and to Janine Rymer, Lisa Bromley and Professors Andrew Strang and William Banks for all their hard work in putting together such a fine conference. My venture into creep is recent and I have benefited from discussions in which I have been able to draw on the vast experience and knowledge of Fujio Abe, Horst Cerjak, Roger Conroy, Sir Alan Cottrell, David Gooch, Masaki Igarashi, Kazuhiro Kimura, Fujimitsu Masuyama, Karl-Heinz Mayer, Bernie Schaffernack, Andrew Strang and Rod Vanstone. My colleagues David Cole, Tracey Cool, Sree Harsha Lalam, Colin Humphreys, Kazutoshi Ichikawa, Joe Robson, Rachel Thomson and David MacKay have been an enormous inspiration and it has been a pleasure to be able to acknowledge their contributions throughout this paper.

REFERENCES

1) C. A. Parsons: The Steam Turbine, Rede Lecture, Cambridge University Press, Cambridge, (1911).
2) D. V. Thronton and K.-H. Mayer: Advances in turbine materials, design and manufacturing, 4th Int. Charles Parsons Turbine Conf., ed. by A. Strang, W. M. Banks, R. D. Conroy and M. J. Goulette, The Institute of Materials, London, (1997), 270.
3) J. F. Knott: Two steps from disaster—the science and engineering of structural integrity, Special Lecture, The Royal Society and Royal Academy of Engineering, London, (1999).
4) T. Fujita: New Steels for Advanced Plant up to to 620 °C, ed. by E. Metcalfe, EPRI, Palo Alto, CA, (1995), 190.
5) F. Masuyama and T. Yokoyama: High Temperature Materials for Power Engineering, ed. by D. Coutsouradis *et al.*, Kluwer Academic Publishers, Dordrecht, (1994), 301.
6) H. Mimura, M. Ohgami, H. Naoi and T. Fujita: High Temperature Materials for Power Engineering, ed. by E. Bachelet *et al.*, Kluwer Academic Publishers, Dordrecht, (1990), 485.
7) H. Cerjak, P. Hofer and B. Schaffernak: *ISIJ Int.*, **39** (1999), 874.
8) J. Hald: New Steels for Advanced Plant up to to 620 °C, ed. by E. Metcalfe, EPRI, Palo Alto, CA, (1995), 152.
9) W. Gelletly: *Philos. Trans. R. Soc. Lond. A*, **356** (1998), 1951.
10) A. H. Cottrell: *European Review*, **1** (1993), 169.
11) A. H. Cottrell: Electron Theory in Alloy Design, ed. by D. G. Pettifor and A. H. Cottrell, The Institute of Materials, London, (1992), 1.
12) M. W. Finnis: Electron Theory in Alloy Design, ed. by D. G. Pettifor and A. H. Cottrell, The Institute of Materials, London, (1992), 10.
13) F. Ducastelle: Electron Theory in Alloy Design, ed. by D. G. Pettifor and A. H. Cottrell, The Institute of Materials, London, (1992), 122.
14) M. Morinaga, R. Hashizume and Y. Murata: Materials for Advanced Power Engineering, Part I, Kluwer Academic Publishers, Dordrecht, (1994), 319.
15) Y. Murata, M. Morinaga and R. Hashizume: Advances in turbine materials, design and manufacturing, 4th Int. Charles Parsons Turbine Conference, ed. by A. Strang, W. M. Banks, R. D. Conroy and M. J. Goulette, The Institute of Materials, London, (1997), 270.
16) A. H. Cottrell: Chemical Bonding in Transition Metal Carbides, The Institute of Materials, London, (1995), 1.
17) F. Brun, T. Yoshida, J. D. Robson, V. Narayan and H. K. D. H. Bhadeshia: *Mater. Sci. Technol.*, **15** (1999), 547.
18) M. Igarashi and Y. Swaragi: Proc. Int. Conf. on Power Engineering–97, JSME, Tokyo, (1997), 107.
19) H. K. D. H. Bhadeshia and L.-E. Svensson: Mathematical Modelling of Weld Phenomena, ed. by K. Easterling and H. Cerjak, The Institute of Materials, London, (1993), 109.
20) H. K. D. H. Bhadeshia: Mathematical Modelling of Weld Phenomena III, ed. by H. Cerjak and H. K. D. H. Bhadeshia, The Institute of Materials, London, (1997), 229.
21) K. Ichikawa, Y. Horii, R. Motomatsu, M. Yamaguchi, and N. Yurioka: *Q. J. Jpn. Weld. Soc.*, **14** (1996), 27.
22) T. Iezawa, T. Inoue, O. Hirano, T. Okazawa and T. Koseki: *Tetsu-to-Hagané*, **79** (1993), 96.
23) E. D. Hyam and J. Nutting: *J. Iron Steel Inst.*, **184** (1956), 148.
24) R. G. Baker and J. Nutting: *J. Iron Steel Inst.*, **192** (1959), 257.
25) G. F. Vander Vroot: Metallography, Principles and Practice, McGraw-Hill Book Company, London, (1984), 219.

26) S. Wignarajah, I. Masumoto and T. Hara: *ISIJ Int.*, **30** (1990), 58.
27) P. M. Anderson, J.-S. Wang and J. R. Rice: Inovations in Ultra-high Strength Steel Technology, ed. by G. B. Olson, M. Azrin and E. S. Wright, Sagamore Army Materials Research Proceedings, NY, (1987), 617.
28) L. P. Sagert, G. B. Olson and D. E. Ellis: *Philos. Mag. B*, **77** (1998), 871.
29) L. P. Zhong, R. Q. Wu, A. J. Freeman and G. B. Olson: *Phys. Rev. B–Condensed Matter*, **55** (1997), 11133.
30) B. E. Wilde, I. Chattoraj and T. A. Mozhi: *Scr. Metall.*, **21** (1987), 1369.
31) M. Igarashi and S. Muneki: Proc. Solid–Solid Phase Transformations '99 (JIMIC-3), ed. by M. Koiwa, K. Otsuka and T. Miyazaki, JIM, Sendai, (1999), 156.
32) C. L. Briant and S. K. Banerji: *Int. Met. Rev.*, **232** (1978), 164.
33) R. Wu, A. J. Freeman and G. B. Olson: *Science*, **265** (1994), 376.
34) M. Hättestrand and H.-O. Andrén: *Mater. Sci. Eng. A*, **A270** (1999), 33.
35) N. Komai, F. Masuyama, I. Ishihara, T. Yokoyama, Y. Yamadera, H. Okada, K. Miyata and Y. Sawaragi: Advanced Heat Resistant Steels for Power Generation, The Institute of Materials, London, (1999), 96.
36) J. Race and H. K. D. H. Bhadeshia: *Mater. Sci. Technol.*, **8** (1992), 875.
37) MTDATA: Metallurgical Thermochemistry Group, National Physical Laboratory, Teddington, London, (1998).
38) S. D. Mann, D. G. McCulloch and B. C. Muddle: *Metall. Mater. Trans. A*, **26A** (1995), 509.
39) J. D. Robson and H. K. D. H. Bhadeshia: *Mater. Sci. Techol.*, **13** (1997), 631.
40) H. K. D. H. Bhadeshia: Proc. Solid–Solid Phase Transformations '99 (JIMIC-3), ed. by M. Koiwa, K. Otsuka and T. Miyazaki, JIM, Sendai, (1999), 1445.
41) J. W. Christian: Theory of Transformations in Metals and Alloys, 2nd ed., part I, Pergamon Press, Oxford, (1975)
42) N. Fujita and H. K. D. H. Bhadeshia: Advanced Heat Resistant Steels for Power Generation, The Institute of Materials, London, (1998).
43) R. G. Baker and J. Nutting: *J. Iron Steel Inst.*, **192** (1959), 257.
44) N. Fujita: Ph.D. thesis, University of Cambridge, (2000).
45) H. K. D. H. Bhadeshia, A. Strang and D. J. Gooch: *Int. Mater. Rev.*, **43** (1998), 45.
46) D. Venugopalan and J. S. Kirkaldy: Hardenability Concepts with Applications to Steels, ed. by D. V. Doane and J. S. Kirkaldy, TMS-AIME, Warrendale, PA, (1978), 249.
47) F. Abe: Proc. 4th Int. Conf. on Recrystallisation and Related Phenomena, ed. by T. Sakai and H. G. Suzuki, JIM, Sendai, (1999), 289.
48) K. Kimura, H. Kushima, F. Abe, K. Yagi and H. Irie: 4th Int. Charles Parsons Turbine Conf., ed. by A. Strang, W. M. Banks, R. D. Conroy and M. J. Goulette, The Institute of Materials, London, (1997), 257.
49) H. K. D. H. Bhadeshia: Proc. of Ultra-Steel 2000, National Research Institute for Metals, Tsukuba, (2000), 205.
50) H. K. D. H. Bhadeshia: *Met. Sci.*, **16** (1982), 159.
51) D. Cole, C. Martin-Moran, A. Sheard, H. K. D. H. Bhadeshia and D. J. C. MacKay: *Sci. Technol. Weld. Joining*, **5** (2000), 81.
52) R. W. K. Honeycombe: *Met. Sci.*, **14** (1980), 201.
53) R. G. Davies and C. L. Magee: *Metall. Trans.*, **2** (1971), 1947.
54) R. G. Davies and C. L. Magee: *Metall. Trans.*, **1** (1970), 2931.
55) S. B. Singh and H. K. D. H. Bhadeshia: *Mater. Sci. Eng. A*, **A245** (1998), 79.
56) D. J. C. MacKay: Mathematical Modelling of Weld Phenomena 3, ed. by H. Cerjak and H. K. D. H. Bhadeshia, The Institute of Materials, London, (1997), 359.
57) H. K. D. H. Bhadeshia: *ISIJ Int.*, **39** (1999), 966.
58) D. J. C. MacKay: *Neural Computation*, **4** (1992), 415.
59) H. K. D. H. Bhadeshia: Bainite in Steels, The Institute of Materials, London, (1992), 1.
60) H. K. D. H. Bhadeshia: Trends in Welding Research, ed. by S. A. David, T. DebRoy, J. A. Johnson, H. B. Smartt and J. M. Vitek, ASM Int., Materials Park, OH, (1999), 795.
61) H. Morimoto, S. Ohkita, H. Sakurai and T. Miyake: Proc. 6th Int. Symp. JWS, JWS, Tokyo, (1996), 405.
62) H. K. D. H. Bhadeshia: Modelling of Microstructural Evolution in Creep Resistant Materials, ed. by A. Strang and M. McLean, The Institute of Materials, London, (1999), 15.
63) F. S. Buffington, K. Hirano and M. Cohen: *Acta Metall.*, **9** (1961), 434.
64) R. J. Borg and C. E. Birchenall: *Trans. TMS-AIME*, **218** (1960), 980.
65) Y. Iijima, K. Kimura and K. Hirano: *Acta Metall.*, **36** (1988), 2811.
66) K. Hirano, M. Cohen and B. L. Averbach: *Acta Metall.*, **9** (1961), 440.
67) J. Kučera: *Czech. J. Phys.*, **B29** (1979), 797.
68) B. Jönsson: *Z. Metallkd.*, **83** (1992), 349.